

## Article

# Combined Cubature Kalman and Smooth Variable Structure Filtering Based on Multi-Kernel Maximum Correntropy Criterion for the Fully Submerged Hydrofoil Craft

Hongmin Niu <sup>1,\*</sup> and Sheng Liu <sup>2</sup> <sup>1</sup> School of Electronics and Control Engineering, Chang'an University, Xi'an 710064, China<sup>2</sup> College of Intelligent Systems Science and Engineering, Harbin Engineering University, Harbin 150001, China; liu.sch@163.com

\* Correspondence: niuhongmin@chd.edu.cn

**Abstract:** This paper introduces a novel filter algorithm termed as an MKMC-CSVSF which combined square-root cubature Kalman (SR-CKF) and smooth variable structure filtering (SVSF) under multi-kernel maximum correntropy criterion (MKMC) for accurately estimating the state of the fully submerged hydrofoil craft (FSHC) under the influence of uncertainties and multivariate heavy-tailed non-Gaussian noises. By leveraging the precision of the SR-CKF and the robustness of the SVSF against system uncertainties, the MKMC-CSVSF integrates these two methods by introducing a time-varying smooth boundary layer along with multiple fading factors. Furthermore, the MKMC is introduced for the adjustment of kernel bandwidths across different channels to align with the specific noise characteristics of each channel. A fuzzy rule is devised to identify the appropriate kernel bandwidths to ensure filter accuracy without undue complexity. The precision and robustness of state estimation in the face of heavy-tailed non-Gaussian noises are improved by modifying the SR-CKF and the SVSF using a fixed-point approach based on the MKMC. The experimental results validate the efficacy of this algorithm.

**Keywords:** multi-kernel maximum correntropy criterion; square-root cubature Kalman filter; smooth variable structure filter; fully submerged hydrofoil craft



**Citation:** Niu, H.; Liu, S. Combined Cubature Kalman and Smooth Variable Structure Filtering Based on Multi-Kernel Maximum Correntropy Criterion for the Fully Submerged Hydrofoil Craft. *Appl. Sci.* **2024**, *14*, 3952. <https://doi.org/10.3390/app14093952>

Academic Editor: José A. Orosa

Received: 11 April 2024

Revised: 30 April 2024

Accepted: 3 May 2024

Published: 6 May 2024



**Copyright:** © 2024 by the authors. Licensee MDPI, Basel, Switzerland. This article is an open access article distributed under the terms and conditions of the Creative Commons Attribution (CC BY) license (<https://creativecommons.org/licenses/by/4.0/>).

## 1. Introduction

The accurate estimation of system states with process and measurement noise is a topic of significant interest for extracting precise state information from available measurements to facilitate subsequent control design. Filters are essential tools in various domains, including utilization in industry and research fields such as signal processing, trajectory tracking, and fault diagnosis. Kalman made a notable contribution to Bayesian filtering, which minimizes the posteriori state error covariance matrix to provide optimal state estimation for state-space models with linear dynamics and Gaussian noises [1]. However, it is crucial to emphasize that exact system information and adherence to Gaussian conditions are prerequisites for optimal performance. Moreover, model approximation errors during filtering can lead to divergence when dealing with nonlinear systems. Consequently, the development and study of alternative nonlinear filtering methods are proposed, such as an extended Kalman filter (EKF), unscented Kalman filter (UKF), and particle Kalman filter (PF) [2–4].

The EKF utilizes the traditional Kalman filter strategy by linearizing the state function through Taylor expansion [5]. However, this method may suffer from error accumulation and decreased accuracy due to strong nonlinearities. The PF approximates posterior probability density using weighted random sample points based on the Monte Carlo sampling method and Bayesian theory [6,7]. Nevertheless, multiple iterations can lead to increased covariance of weight and particle degeneracy with local optimization. The UKF employs

a scaled unscented transformation process and deterministic sampling technique to approximate the posteriori probability density with higher precision [8,9]. However, the artificial selection of parameters may impact the filtering performance. Recently, the most numerically stable and accurate cubature Kalman filter (CKF) has been introduced [10]. The CKF approximates multi-dimensional integrals in Bayesian filtering under a Gaussian assumption, offering advantages such as rigorous theoretical derivation, third-order filtering accuracy, and reliable stability [11,12]. The CKF is extensively employed in applications like spacecraft attitude estimation and trajectory tracking due to its higher estimation precision and convergence rate for high-dimension systems [13,14]. Nevertheless, computational inaccuracies and the limited word length of the computers may result in the state error covariance of CKF losing the property of being symmetric positive definite, which can ultimately lead to divergence. To prevent divergence while maintaining positive specificity, the square-root cubature Kalman (SR-CKF) has been developed, transmitting both the predicted and the posteriori square roots of error covariance to avoid negativity in the covariance matrix in iterations [15,16].

In practical situations, system parameters may be drastically impacted by faults or external disturbances, leading to uncertainties and potential degradation and instability in common filters. Moreover, it is difficult to determine information on these modeling uncertainties. Thus, to deal with modeling errors and system uncertainties, robust estimation methods and adaptive state estimations have been proposed. The  $H_\infty$  filter is designed by reducing the extreme scenario estimation discrepancies, while it is sensitive to the quantity of weighting functions and performance boundaries defined by users [17,18]. On the other hand, an innovative and robust estimation strategy termed as a smooth variable structure filter (SVSF) has been introduced [19–21]. It is a robust iterative estimation refinement method based on the smooth variable structure principles that enhances the robustness and stability by effectively managing modeling uncertainties. Combining the SVSF with the EKF or UKF has been suggested to improve robustness of the system uncertainties [22]. Additionally, an algorithm named CSVSF, which combines CKF and SVSF, is proposed [23]. However, these prior works assume a Gaussian measurement noise, neglecting heavy-tailed non-Gaussian noises existing in the system.

To address heavy-tailed non-Gaussian noises and impulsive noises in engineering applications, various methods have been explored. The Huber robust function and information theoretic learning (ITL) are commonly used techniques for filtering non-Gaussian noises. The ITL captures high-order statistics, leading to a direct improvement in filter performance [24,25]. Specifically, the maximum correntropy criterion (MCC) has shown effectiveness in non-Gaussian conditions by maximizing the correntropy between the system output and desired performance [26,27]. Kalman filtering methods based on the MCC have exhibited exceptional performance in impulsive noise scenarios [28–31].

However, challenges related to MCC implementation have been addressed using an efficient fixed-point iterative method [32]. Notably, parameter uncertainties inherent in real-world applications are often overlooked. As the kernel bandwidth significantly influences the presentation of the MCC, the selection of the kernel bandwidth mentioned previously is typically conducted through trial and error by users, which is complex and impacts the accuracy of the filter.

This paper proposes an MKMC-CSVSF which combined the SR-CKF and SVSF under the multi-kernel maximum correntropy criterion (MKMC) to enhance the robustness against lumped uncertainties and heavy-tailed non-Gaussian noises commonly encountered in practical implementations such as a FSHC. The SR-CKF combined with the SVSF by a time-varying smooth boundary layer with multiple fading factors improving the filter's accuracy and exhibiting robust performance against system uncertainties. Moreover, the MKMC is introduced to ensure the robustness in contrast to heavy-tailed non-Gaussian noises across different channels, making it more applicable for practical scenarios. A fuzzy rule is designed to automatically determine the kernel bandwidths.

## 2. Correntropy Criterion

The correntropy evaluates the resemblance of random variables  $X, Y \in R$  and it is calculated based on the joint distribution function  $F_{XY}(x_1, y_1)$ , the correntropy function is specified as follows:

$$V(X, Y) = E(\chi(X, Y)) = \int \int \chi(x_1, y_1) dF_{XY}(x_1, y_1) \tag{1}$$

where  $E(\cdot)$  denotes the expectation operator,  $\kappa(X, Y)$  represents a kernel function with non-negative symmetric properties.  $F_{XY}(x_1, y_1)$  signifies the probability density function of  $X, Y$ . The Gaussian kernel is utilized as the kernel function and its definition is presented as:

$$\chi(x, y) = G_{\bar{\sigma}}(e_{\zeta}) = \frac{1}{\sqrt{2\pi\bar{\sigma}}} \exp\left(-\frac{e_{\zeta}^2}{2\bar{\sigma}^2}\right) \tag{2}$$

where  $e_{\zeta} = x_1 - y_1$  is the difference between  $x$  and  $y$ , and the  $\bar{\sigma} > 0$  denotes the kernel bandwidth of the correntropy function.

In several practical circumstances, data samples are frequently limited and the probability density function is not known. Consequently, the computation of correntropy estimation is performed using a selection of samples:

$$\bar{V}(X, Y) = \frac{1}{\bar{M}} \sum_{i=1}^{\bar{M}} G_{\bar{\sigma}}(e_{\zeta}(i)) \tag{3}$$

where  $e_{\zeta}(i) = x_1(i) - y_1(i), i = 1, 2, \dots, \bar{M}$  are the data samples of the  $F_{XY}(x_1, y_1)$ .

Expanding the Gaussian kernel function, one can obtain:

$$V(X, Y) = \sum_{N=0}^{\infty} \frac{(-1)^N}{2^N \bar{\sigma}^{2N} N!} E[(X - Y)^{2N}] \tag{4}$$

It is clear that the correntropy function can be represented as the sum of moments of the error variable  $X - Y$  with even orders. The kernel bandwidth  $\bar{\sigma}$  is used to allocate weights to higher-order moments. Notably, the second-order moment plays a significant role in determining the correntropy when the kernel bandwidth selected is significantly large [27].

Considering the error sequence  $e_{\zeta}(i)$ , when  $e_{\zeta}(i) = 0$ , the Gaussian kernel function will be the maximum value; the objective function of the MCC is formulated as:

$$L_{MCC} = \min\left(\sum_{i=1}^{\bar{M}} G_{\bar{\sigma}}(0) - G_{\bar{\sigma}}(e_{\zeta}(i))\right) \tag{5}$$

## 3. Estimation Algorithm

### 3.1. Square Root Cubature Kalman Filter

The SVSF is a model-based filter which efficiently manages structural or parametric uncertainty and takes into account the effects of uncertainties and noise in measurements on filter stability and convergence. The purpose of this study is to improve filter precision and resilient performance against parametric uncertainties by combining the SVSF and SR-CKF.

According to the following system, which incorporates a nonlinear process function and a linear measurement equation as:

$$x_k = f(x_{k-1}, u_{k-1}) + w_{k-1} \tag{6}$$

$$z_k = H_k x_k + v_k \tag{7}$$

where  $x_k \in R^n$  denotes the state variable,  $z_k \in R^m$  means the measurement vector, and  $u_{k-1} \in R^n$  represents the control vector. The  $f(\cdot)$  signifies the nonlinear function which is assumed to be differentiable to the states. The term  $w_{k-1}$  refers to the process noise with a covariance of  $Q_k$  and  $v_k$  denotes the measurement noise with a covariance of  $R_k$ . The  $w_{k-1}$  and  $v_k$  are zero-mean Gaussian processes and independent of each other.

The CKF is derived based on the third-order spherical-radial rule to compute the Gaussian weighted integrals. The cubature rule provides an approximation for m-dimensional integrals with Gaussian weights as detailed below [10]:

$$\int_{R^n} f(x)N(x, \mu, P_1)dx \approx \frac{1}{2m} \sum_{i=1}^{2m} f(\mu + \sqrt{P_1}\bar{\xi}_i) \tag{8}$$

where the covariance  $P_1 = \sqrt{P_1}\sqrt{P_1}^T$  and the  $\bar{\xi}_i$  is the  $i$ th element of  $2m$  cubature points as follows:

$$\bar{\xi}_i = \begin{cases} \sqrt{m}\bar{e}_i, i = 1, 2, \dots, m \\ -\sqrt{m}\bar{e}_{i-n}, i = n + 1, n + 2, \dots, 2m \end{cases} \tag{9}$$

$$\bar{e} = \left\{ \begin{pmatrix} 1 \\ 0 \\ \vdots \\ 0 \end{pmatrix}, \begin{pmatrix} 0 \\ 1 \\ \vdots \\ 0 \end{pmatrix}, \dots, \begin{pmatrix} 0 \\ \vdots \\ 0 \\ 1 \end{pmatrix}, \begin{pmatrix} -1 \\ 0 \\ \vdots \\ 0 \end{pmatrix}, \begin{pmatrix} 0 \\ -1 \\ \vdots \\ 0 \end{pmatrix}, \dots, \begin{pmatrix} 0 \\ \vdots \\ 0 \\ -1 \end{pmatrix} \right\} \tag{10}$$

where  $\bar{e}_i$  means the  $i$ -th element of  $\bar{e}$ . It represents the  $i$ -th elementary column vector. Given the benefits of using the square-root form of the CKF, which includes assured covariance properties and a prevention of estimation error covariance divergence, the SR-CKF is employed in this study.

Firstly, the state and error covariance are initialized. The Cholesky decomposition is used to calculate the error covariance matrix and measurement noise:

$$P_{k-1|k-1} = S_{k-1|k-1}S_{k-1|k-1}^T \tag{11}$$

$$S_{Q,k-1} = Chol(Q_k) \tag{12}$$

The SR-CKF methodology encompasses a time update phase and a measurement update phase. The process of implementing the SR-CKF is outlined.

Step 1: The time update stage is designed to predict the state at the next time step based on the dynamic model of the system.

Determining the cubature points and advancing them by the state function:

$$X_{i,k-1} = S_{k-1}\bar{\xi}_i + \hat{x}_{k-1} \tag{13}$$

$$X^*_{i,k} = f(X_{i,k-1}) \tag{14}$$

Then, calculating the state prediction and the square-root of the predicted state error covariance:

$$\hat{x}_{k|k-1} = \sum_{i=1}^{2m} \omega_i X^*_{i,k} \tag{15}$$

$$S_{k|k-1} = Tria([\chi^*_{k|k-1} \quad S_{Q,k-1}]) \tag{16}$$

$$\chi^*_{k|k-1} = \frac{1}{\sqrt{2m}} [X^*_{1,k|k-1} - \hat{x}_{k|k-1} \quad X^*_{2,k|k-1} - \hat{x}_{k|k-1} \quad X^*_{3,k|k-1} - \hat{x}_{k|k-1} \quad \dots \quad X^*_{2n,k|k-1} - \hat{x}_{k|k-1}] \tag{17}$$

Step 2: The measurement update stage utilizes new measurement data to correct the predicted state, thereby obtaining more precise estimations.

Cubature points are established and propagated through the measurement function to refine the predicted state and measurement estimates as follows:

$$X_{i,k|k-1} = S_{k|k-1}\zeta_i + \hat{x}_{k|k-1} \tag{18}$$

$$Z_{i,k|k-1} = HX_{i,k|k-1} \tag{19}$$

The measurement predictive estimation is derived as:

$$\hat{z}_{k|k-1} = \sum_{i=1}^{2n} \omega_i Z_{i,k|k-1} \tag{20}$$

Then the square-root of the measurement error covariance and the covariance matrix are shown as:

$$S_{zz,k|k-1} = \text{Tri}a([\gamma_{k|k-1}^* \quad S_{R,k-1}]) \tag{21}$$

$$P_{xz,k|k-1} = \tilde{\chi}_{k|k-1} \tilde{\gamma}_{k|k-1}^T \tag{22}$$

$$\tilde{\gamma}_{k|k-1} = \frac{1}{\sqrt{2n}} [Z_{1,k|k-1} - \hat{z}_{k|k-1} \quad Z_{2,k|k-1} - \hat{z}_{k|k-1} \quad Z_{3,k|k-1} - \hat{z}_{k|k-1} \quad \cdots \quad Z_{2n,k|k-1} - \hat{z}_{k|k-1}] \tag{23}$$

$$\tilde{\chi}_{k|k-1} = \frac{1}{\sqrt{2n}} [X_{1,k|k-1} - \hat{x}_{k|k-1} \quad X_{2,k|k-1} - \hat{x}_{k|k-1} \quad X_{3,k|k-1} - \hat{x}_{k|k-1} \quad \cdots \quad X_{2n,k|k-1} - \hat{x}_{k|k-1}] \tag{24}$$

where  $\text{Tri}a(\cdot)$  is subjected to a triangularization process in order to produce a lower triangular matrix. The filter gain matrix, state estimation, and square-root error covariance matrix of time are computed in the following manner and utilized in the subsequent stage of an iterative procedure.

$$K_k = (P_{xz,k|k-1} / S_{zz,k|k-1}) / S_{zz,k|k-1}^T \tag{25}$$

$$\hat{x}_{k|k} = \hat{x}_{k|k-1} + K_k(z_{k|k-1} - \hat{z}_{k|k-1}) \tag{26}$$

$$S_{k|k} = \text{Tri}a([\chi_{k|k-1} - K_k \gamma_{k|k-1} \quad K_k S_{R,k}]) \tag{27}$$

### 3.2. Combined SR-CKF and SVSF

To strengthen the system's reliability of the SR-CKF against system uncertainties in the practical applications. An algorithm that combines the SR-CKF with an SVSF is defined as CSVSF and the procedure is summarized as follows [23].

Initially, the SVSF is presented through the integration of the principles of a variable structure concept and sliding mode theory.

$$\hat{x}_{k|k-1} = f(\hat{x}_{k-1|k-1}, u_{k-1}) \tag{28}$$

$$P_{k|k-1} = B_{k-1} P_{k-1|k-1} B_{k-1}^T + Q_{k-1} \tag{29}$$

$$B_{k-1} = \left. \frac{\partial f}{\partial x} \right|_{x_{k-1|k-1}} \tag{30}$$

The predicted measurement and measurement errors of the SVSF are gained as:

$$\hat{z}_{k|k-1} = H_{k-1} \hat{x}_{k|k-1} \tag{31}$$

$$\hat{e}_{z,k|k-1} = z_k - \hat{z}_{k|k-1} \tag{32}$$

Subsequently, the SVSF gain can be determined by taking into account both the initial measurement error  $\widehat{e}_{z,k-1|k-1}$  and the updated measurement error  $e_{z,k|k-1}$ .

$$\overline{K}_k = H^+_k \text{diag} \left[ \left( \left| \widehat{e}_{z,k|k-1} \right| + \lambda \left| \widehat{e}_{z,k-1|k-1} \right| \right) \circ \text{sat}(\varphi^{-1} \widehat{e}_{z,k|k-1}) \right] \text{diag}^{-1}(\widehat{e}_{z,k|k-1}) \quad (33)$$

where  $H^+_k$  denotes the pseudoinverse of the measurement matrix,  $\lambda$  represents the convergence rate,  $\circ$  means the Schur multiplication, and  $\varphi$  denotes the boundary layer of the SVSF.

To mitigate the emergence of excessive noise, the saturation function, which includes an optimal boundary layer, is employed instead of the sign function. The saturation function is defined as:

$$\text{sat}(\varphi^{-1} \widehat{e}_{z,k|k-1}) = \begin{cases} 1, & \varphi_i^{-1} \widehat{e}_{z_i,k|k-1} \geq 1 \\ \varphi_i^{-1} \widehat{e}_{z_i,k|k-1}, & -1 \leq \varphi_i^{-1} \widehat{e}_{z_i,k|k-1} \leq 1 \\ -1, & \varphi_i^{-1} \widehat{e}_{z_i,k|k-1} \leq -1 \end{cases} \quad (34)$$

As the boundary layers are coupled to each other, to achieve a more precise state estimation, a coupled smooth boundary layer matrix is introduced, which encompasses interconnected boundary layers:

$$\overline{\varphi} = \begin{bmatrix} \varphi_{11} & \varphi_{12} & \cdots & \varphi_{1m} \\ \varphi_{21} & \varphi_{22} & \cdots & \varphi_{2m} \\ \vdots & \vdots & \ddots & \vdots \\ \varphi_{m1} & \varphi_{m2} & \cdots & \varphi_{mm} \end{bmatrix} \quad (35)$$

The derivation of the predictive covariance to the boundary layer enables the attainment of an ideal boundary layer [22]:

$$\frac{\partial(\text{trace}[P_{k-1|k-1}])}{\partial \varphi} = 0 \quad (36)$$

According to [20], the smoothing boundary needs to exceed the uncertain dynamics of the system to maintain the stability and eliminate the chattering. Nevertheless, employing a much broader width for the SVSF could result in slower convergence and performance degradation. Therefore, we can determine the optimal boundary layer of the CSVSF by employing the following calculation method:

$$\varphi_k = (\overline{\psi}^{-1} H_{k-1} \overline{P}_{k|k-1} H^T_{k-1} F^{-1}_k)^{-1} \quad (37)$$

$$\overline{\psi} = \left( \left| e_{k|k-1} \right| + \delta \left| e_{k-1|k-1} \right| \right) \quad (38)$$

where  $\overline{\psi}$  is the diagonal matrix of  $\psi$ . Revisions are applied to both the state estimate and its error covariance matrix, resulting in:

$$\hat{x}_{k|k} = \hat{x}_{k|k-1} + \overline{K}_k e_{z,k|k-1} \quad (39)$$

$$\overline{P}_{k|k} = (I - K_k H_{k-1}) \overline{P}_{k|k-1} (I - K_k H_{k-1})^T + K_k R_k K^T_k \quad (40)$$

Ultimately, the measurement estimate and the measurement error are calculated:

$$\hat{z}_{k|k} = H_k \hat{x}_{k|k} \quad (41)$$

$$e_{z,k|k} = z_k - \hat{z}_{k|k} \quad (42)$$

Considering the relationship between the SR-CKF and the SVSF through the implementation of a smooth boundary layer in the SVSF, it is observed that a wider constant smoothing boundary layer width compared to the time-varying one may lead to inaccuracies in the SVSF. Therefore, the SR-CKF is employed to optimize the accuracy of the filter. To address discrepancies between the constant and time-varying smoothing boundaries and ensure filter stability, the SVSF is utilized when the time-varying boundary extends beyond the constant one. The state trajectory of the CSVSF considering the influence of disturbances is shown in Figure 1.

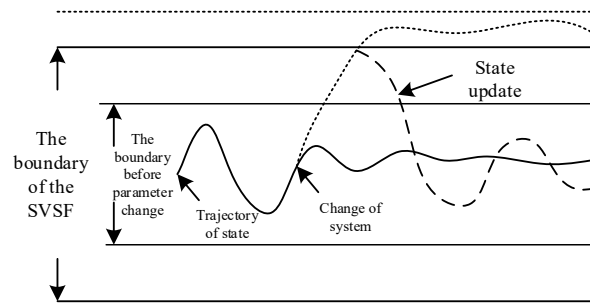


Figure 1. The state trajectory of the CSVSF.

#### 4. The CSVSF Based on Multi-Kernel Maximum Correntropy Criterion

It is widely recognized that the presented filtering algorithm may suffer from a decrease in performance when confronting non-Gaussian disturbances. The CSVSF algorithm is improved to better withstand external disturbances and heavy-tailed non-Gaussian noise by integrating the MKMC criterion, which considers higher-order moments of errors. Thus, the algorithm proposed achieves high filtering accuracy and robustness against parametric uncertainties and heavy-tailed non-Gaussian noise simultaneously [28].

According to the discrete-time system (6) and (7), which may operate in heavy-tailed non-Gaussian noise and external disturbances, we can obtain:

$$\begin{bmatrix} \hat{x}(k|k-1) \\ z(k) \end{bmatrix} = \begin{bmatrix} I \\ H(k) \end{bmatrix} x(k) + \zeta(k) \tag{43}$$

where  $I$  denotes the unit matrix of  $n \times n$ ,  $\delta(k)$  is defined as:

$$\zeta(k) = \begin{bmatrix} -x(k) - \hat{x}(k|k-1) \\ v(k) \end{bmatrix} \tag{44}$$

$$\begin{aligned} \Phi(k) &= E[\zeta(k)\zeta^T(k)] = \begin{bmatrix} P(k|k-1) & 0 \\ 0 & R(k) \end{bmatrix} \\ &= \begin{bmatrix} S_{k|k-1}S_{k|k-1}^T & 0 \\ 0 & S_{R,k}S_{R,k}^T \end{bmatrix} = A(k)A^T(k) \end{aligned} \tag{45}$$

$A(k)$  is gained by the Cholesky decomposition of the  $E[\zeta(k)\zeta^T(k)]$ . Then, multiplying both sides of (45) by  $A^{-1}(k)$ , one can obtain:

$$B(k) = C(k)x(k) + \tilde{\zeta}(k) \tag{46}$$

$$B(k) = A^{-1}(k) \begin{bmatrix} \hat{x}(k|k-1) \\ z(k) \end{bmatrix}, C(k) = A^{-1}(k) \begin{bmatrix} I \\ H(k) \end{bmatrix}, \tilde{\zeta}(k) = A^{-1}(k)\zeta(k) \tag{47}$$

The MKMC-based cost function is gained considering the multiple kernel bandwidths:

$$J_{(n+m)}(x(k)) = \frac{1}{(n+m)} \sum_{i=1}^{n+m} G_{\sigma_i} [b_i(k) - c_i(k)x(k)] \tag{48}$$

$G_{\sigma_i}(e_{i,k})$  denotes the Gaussian function with the kernel bandwidth  $\sigma_i$ ,  $b_i(k)$  means the  $i$ th item of  $B(k)$ ,  $c_i(k)$  represents the  $i$ th item of  $C(k)$ , and  $\xi_i(k) = b_i(k) - c_i(k)x(k)$  means the error at time step  $k$ . The optimal estimation of the state is obtained:

$$\hat{x}(k) = \operatorname{argmax}_{x(k)} J_{(n+m)}(x(k)) = \frac{1}{(n+m)} \sum_{i=1}^{n+m} G_{\sigma_i}(\xi_i(k)) \tag{49}$$

Differentiating the (48), we can establish that:

$$\frac{\partial J_{(n+m)}(x(k))}{\partial x(k)} = 0 \tag{50}$$

Substituting the (2) into (50), then the function with multiple kernel bandwidths is gained:

$$\sum_{i=1}^{n+m} G_{\sigma_i}(e_i(k)) \cdot \xi_i(k) \frac{\partial \xi_i(k)}{\partial x(k)} = 0 \tag{51}$$

Defining  $G_{\sigma_i}(\xi_i(k)) \cdot \xi_i(k) = \eta(\xi_i(k))$ , then  $\eta(\xi_i(k)) / \xi_i(k) = d_i(k)$ , the Function (51) can be expressed as:

$$\left( \frac{\partial \xi(k)}{\partial x(k)} \right)^T D(k) [B(k) - C(k)x(k)] = 0 \tag{52}$$

where  $D(k)$  is defined as  $D(k) = \begin{bmatrix} D_x(k) & 0 \\ 0 & D_z(k) \end{bmatrix}$  for convenience.  $D_x(k) = \operatorname{diag}(G_{\sigma_1}(\xi_1(k)), \dots, G_{\sigma_n}(\xi_n(k)))$ ,  $D_z(k) = \operatorname{diag}(G_{\sigma_{n+1}}(\xi_{n+1}(k)), \dots, G_{\sigma_{n+m}}(\xi_{n+m}(k)))$ . The  $\sigma_1, \sigma_2, \dots, \sigma_{n+m}$  mean multi-kernel bandwidths.  $\sigma_1, \sigma_2, \dots, \sigma_n$  denote the bandwidths of the system process.  $\sigma_{n+1}, \sigma_{n+2}, \dots, \sigma_{n+m}$  are the bandwidths of the measurement.

Therefore, the modified covariance is gained as  $\tilde{\Phi}(k) = A(k)D(k)A^T(k)$ ; for the sake of analysis, the  $\tilde{\Phi}(k)$  is modified to diagonal form:

$$\tilde{\Phi}(k) = \begin{bmatrix} \tilde{\Phi}_x(k) & 0 \\ 0 & \tilde{\Phi}_z(k) \end{bmatrix} \tag{53}$$

Given the challenge in ascertaining the system state, the  $x(k)$  is assumed equal to  $\hat{x}(k|k-1)$ , thus:

$$\tilde{\Phi}_x(k) = S_{k|k-1} \cdot D_x(k) \cdot S_{k|k-1}^T = \tilde{P}(k|k-1) \tag{54}$$

Meanwhile, the noise covariance is modified as:

$$\tilde{\Phi}_z(k) = \tilde{R}(k) = \tilde{S}_R(k)D_z(k)\tilde{S}_R^T(k) \tag{55}$$

**Remark 1.** It is clear that the option for the kernel bandwidth significantly influences the effectiveness of the MKMC. Choosing a smaller kernel bandwidth can enhance the algorithm’s robustness against outliers. However, excessively small values can lead to filter divergence or deterioration. Conversely, selecting a significantly larger kernel bandwidth renders the MKMC ineffective, reverting the algorithm to its original filter state. Previous studies [29] have relied on trial-and-error methods for choosing the kernel bandwidth, which can be complex and time-consuming. To address this issue, we suggest automatically adjusting the kernel bandwidth using fuzzy rules to achieve an adaptive kernel bandwidth.

Consequently, the algorithmic process of MKMC-CSVSF which combines the SR-CKF and the SVSF based on the MKMC can be outlined as follows:

- (1) Determine the cubature point and propagate it with respect to the state function by (13) and (14).
- (2) Calculating the priori state estimate and the square-root covariance matrix through (15) and (16).

- (3) Calculating the measurement predictive estimation through the estimate function as (19), (20).
- (4) Considering the MKMC, calculate the modified noise covariance  $\tilde{R}(k)$  by (43)–(55).
- (5) Then, considering the MKMC, and the modified measurement covariance in (21), the state error covariance of the SR-CKF in (27) and the state error covariance of the SVSF in (40) are used to replace the original measurement covariance for the robust to the heavy-tailed outliers.

$$S_{zz,k|k-1} = \text{Tri}([\gamma_{k|k-1} \quad \tilde{S}_{R,k-1}]) \tag{56}$$

$$S_{k|k} = \text{Tri}([\chi_{k|k-1} - K_k \gamma_{k|k-1} \quad K_k \tilde{S}_{R,k}]) \tag{57}$$

$$P_{SVSF,k|k} = (I - K_{SVSF,k} H_{k-1}) P_{SVSF,k|k-1} (I - K_{SVSF,k} H_{k-1})^T + K_{SVSF,k} \tilde{R}_{SVSF,k} K_{SVSF,k}^T \tag{58}$$

- (6) Then, the predicted state estimation and state error covariance are obtained as (26), (27).
- (7) Calculating the predicted measurement in (31), measurement errors in (32) and the gain of the SVSF in (33).
- (8) Comparing the constant and time-varying layer, in the event that the fixed boundary layer’s width surpasses the width of its time-varying counterpart, the SR-CKF based on the MKMC is used to refine the precision of the filter. The filter gain matrix and the modified state estimation are calculated as (25), (26). When the width of the time-varying smoothing boundary layer exceeds that of the constant one, the SVSF based on the MKMC is utilized to confirm a reliable estimate. The filter gain matrix and the modified state estimation are calculated as (39), (40).
- (9) Then, update the measurement estimate and estimation error as (41), (42).

**Remark 2.** *Consequently, it can be deduced that the MKMC-CSVSE, as proposed in this study, exhibits improved precision and robust performance in dealing with uncertain dynamics and heavy-tailed non-Gaussian noises. By setting the kernel bandwidths to a specific value as  $\sigma_i \rightarrow \infty$ , the MKMC-CSVSE is converted to the conventional CSVSE, which effectively handles Gaussian noises and uncertain dynamics. Conversely, when different kernel bandwidths are employed as  $\sigma_i = \sigma$ , the proposed filter reverts back to the CSVSE based on the MCC. Remarkably, this novel MKMC-CSVSE approach not only mitigates Gaussian noise but also attenuates non-Gaussian noise simultaneously. It outperforms the CKF and CSVSE under conditions where dynamic uncertainties coexist with heavy-tailed noises. Therefore, the algorithm proposed holds significant practical applicability and can be widely used in a practical condition.*

### 5. Results

The proposed method is tested on two scenarios to demonstrate its effectiveness, which includes a standard one-dimensional case and the state estimation of a fully submerged hydrofoil craft (FSHC). Statistical metrics like a mean squared error (MSE) and average mean squared error (AMSE) are computed to evaluate the algorithms’ performance:

$$RMSE_1(i) = \sqrt{\frac{1}{K} \sum_{k=1}^K (x(k) - \hat{x}(k|k))^2}, i = 1, 2 \dots \Upsilon \tag{59}$$

$$ARMSE = \frac{1}{\Upsilon} \sum_{i=1}^{\Upsilon} RMSE_1(i) \tag{60}$$

where  $K$  is the time steps and  $\Upsilon$  is the number of Monte Carlo runs.

5.1. Example 1

Firstly, we examine the one-dimensional example which serves as a univariate nonstationary growth model commonly employed in nonlinear filtering. The system is depicted as follows:

$$x_1(k) = a_1x_1(k - 1) + a_2\frac{x_1(k - 1)}{1 + x_1(k - 1)^2} + a_3\cos(1.2(k - 1)) + w_1(k - 1) \quad (61)$$

$$z_1(k) = \frac{x_1^2(k)}{20} + v_1(k) \quad (62)$$

The parameters are selected as  $a_1 = 0.5$ ,  $a_2 = 2.5$ ,  $a_3 = 8$ ,  $K = 100$  and  $\Upsilon = 100$ . The convergence rate in the MKMC-CSVSF filter gain is selected as  $\lambda = 0.1$ . The kernel bandwidth of the MKMC criterion is selected as  $\sigma = 5$ .

Firstly, the system and measurement noises are characterized by a Gaussian probability functions as  $w_1(k - 1) \sim N(0, 0.06)$ ,  $v_1(k) \sim N(0, 0.01)$ . Then the ARMSE of various algorithms including the CKF, CSVSF and MKMC-CSVSF are calculated and presented in Table 1.

**Table 1.** ARMSEs of  $x_1$  with Gaussian noise.

Filter Algorithm	ARMSE of $x$
CKF	0.1788
CSVSF	0.2110
MKMC-CSVSF (Fuzzy rule)	0.1953
MKMC-CSVSF ( $\sigma = 0.5$ )	0.2410
MKMC-CSVSF ( $\sigma = 2$ )	0.2347
MKMC-CSVSF ( $\sigma = 5$ )	0.2605
MKMC-CSVSF ( $\sigma = 10$ )	0.2209

Then, considering the dynamic uncertainties, the parameter  $a_3 = 8$  is changed to  $a_3 = 4$  at  $K = 50$  during each Monte Carlo simulation. Meanwhile, the measurement error is substituted with a heavy-tailed non-Gaussian distribution, under the assumption that the measurement errors adhere to a mixed-Gaussian distribution  $w_1(k - 1) \sim N(0, 0.06)$ ,  $v_1(k) \sim 0.8N(0, 0.01) + 0.2N(0, 10)$ . The statistical results are presented in Table 2 in this scenario.

**Table 2.** ARMSEs of  $x_1$  with non-Gaussian noise.

Filter Algorithm	ARMSE of $x$
CKF	0.5889
CSVSF	0.5409
MKMC-CSVSF (Fuzzy rule)	0.2876
MKMC-CSVSF ( $\sigma = 0.5$ )	0.3054
MKMC-CSVSF ( $\sigma = 2$ )	0.3257
MKMC-CSVSF ( $\sigma = 5$ )	0.3559
MKMC-CSVSF ( $\sigma = 10$ )	0.3932

Hence, according to the aforementioned results, it is apparent that if the system and measurement noises are characterized by Gaussian statistics, the presentation of the CKF, CSVSF and the proposed MKMC-CSVSF demonstrates similar levels of accuracy in state estimation. However, in scenarios where non-Gaussian heavy-tailed noise coexists with system uncertainties, the proposed MKMC-CSVSF algorithm outperforms the other two methods. The ARMSE of the MKMC-CSVSF exhibits notably lower values and provides more accurate state estimation. Moreover, it is worth noting that the fuzzy rule employed for selecting the kernel bandwidth proves to be effective and optimal. This optimal se-

lection of the kernel bandwidth mitigates filtering divergence issues while improving filtering accuracy.

5.2. Example 2

Subsequently, we focus on the estimation of the longitudinal behavior of the fully submerged hydrofoil craft (FSHC). The FSHC’s nonlinear model, encompassing both translational and rotational movements, is constructed on the basis of rigid body dynamics and momentum theorem [33,34]:

$$(Z_{\dot{w}} - m)\dot{w} + Z_w w + Z_z z + Z_{\dot{q}} \dot{q} + (Z_q + U_e m)q + Z_{\theta} \theta = -Z_{\delta_e} \delta_e - Z_{\delta_f} \delta_f - Z_S \quad (63)$$

$$M_{\dot{w}} \dot{w} + M_w w + M_z z + (M_{\dot{q}} - I_y) \dot{q} + M_q q + M_{\theta} \theta = -M_{\delta_e} \delta_e - M_{\delta_f} \delta_f - M_S \quad (64)$$

$$\begin{bmatrix} \dot{z} \\ \dot{\theta} \end{bmatrix} = \begin{bmatrix} \cos \theta & 0 \\ 0 & 1 \end{bmatrix} \begin{bmatrix} w \\ q \end{bmatrix} + \begin{bmatrix} -U_e \sin \theta \\ 0 \end{bmatrix} \quad (65)$$

where  $\begin{bmatrix} \dot{z} \\ \dot{\theta} \end{bmatrix}$  refers to the velocity of the vertical movement and the velocity of the pitch angle in an earth-fixed frame,  $\begin{bmatrix} w \\ q \end{bmatrix}$  holds an equivalent interpretation in the body-fixed coordinate, and  $U_e$  is the steady speed of the FSHC. The means of the variable of (63), (64) can refer to the [31,32]. The nonlinear second-order state space function of the FSHC is designed as:

$$\dot{x}_1 = x_2 \quad (66)$$

$$\dot{x}_2 = f(x_1, x_2) + Bu + DW \quad (67)$$

Equations (66) and (67) are discretized through the application of the fourth-order Runge–Kutta method, resulting in a nonlinear discrete model for the longitudinal behavior of the FSHC, together with a linear measurement function.

$$x_k = f(x_{k-1}, u_{k-1}) + d(t) + w_{k-1} \quad (68)$$

$$z_k = H_k x_k + v_k \quad (69)$$

where  $x_k = [z \quad \dot{z} \quad \theta \quad \dot{\theta}]^T \in R^4$  are the state of the system,  $z_k = [z \quad \theta]^T \in R^2$  represents the measurement state,  $u_k \in R^2$  means the control item, and  $H_k$  denotes the measurement matrix.  $w_k \sim N(0, Q_k)$ ,  $v_k \sim N(0, R_k)$  are the system noises and measurement noises. The system’s simulation duration is defined as  $t = 100$  s with a sampling interval of  $T = 0.1$  s. A total of  $\Upsilon = 50$  Monte Carlo iterations are conducted. The initial states and covariance matrix are specified as  $X_0 = [0.01 \quad 0.01 \quad 0.01 \quad 0.01]^T$ ,  $P_0 = \text{diag}([100 \quad 10 \quad 100 \quad 10])$ . The measurement matrix is  $H_k = \begin{bmatrix} 1 & 0 & 0 & 0 \\ 0 & 0 & 1 & 0 \end{bmatrix}$ . The measurement noise covariance is  $R = \text{diag}([0.06 \quad 0.25])$  and the system noise covariance set as  $Q = \text{diag}([1 \quad 1 \quad 1 \quad 1])$ . The parameters of the FSHC can refer to [33,34].

In this case,  $\delta$  is selected as  $\delta = 0.4 - 0.5$ . The fuzzy rule is as follows:

$$\text{If } \|z_k - \hat{z}_{k|k-1}\| > 0.1, \text{ then decrease the } \rho, \rho = 0.01 \quad (70)$$

$$\text{If } \|z_k - \hat{z}_{k|k-1}\| < 0.1, \text{ then decrease the } \rho, \rho = 400 \quad (71)$$

We assume the fact that the FSHC maintains a constant speed of 45 kn with a significant wave height of 1.5 m and the encounter angles of ocean waves are set at 30°. We further assume that the measurement noise adheres to a non-Gaussian noise distribution as:

$$r_1(k) \sim 0.9N(0, 0.06) + 0.1N(0, 6) \quad (72)$$

$$r_2(k) \sim 0.9N(0, 0.25) + 0.1N(0, 25) \quad (73)$$

In order to validate the competence of the MKMC-CSVSF, the CKF, CSVSF and the MCSVSF are compared in the experiment for the longitudinal behavior estimation of the FSHC.

The estimation performance of the CKF, CSVSF and proposed MKMC-CSVSF for the heave motion of the FSHC is shown in Figure 2 while the corresponding estimation errors are depicted in Figure 3. The results of the estimate and discrepancies for heave velocity are exhibited in Figures 4 and 5, respectively. The estimation results and errors for the pitch angle of the FSHC are displayed in Figures 6 and 7. The estimation results and deviations of the pitch angle velocity are visualized in Figures 8 and 9. The average mean squared error (AMSE) for various filter methods applied to the FSHC are calculated individually.

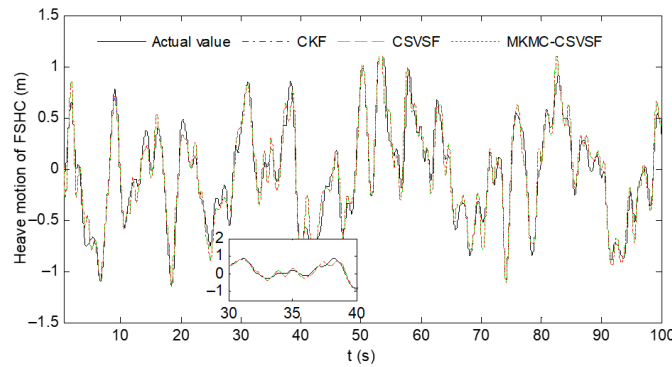


Figure 2. The estimation of heave motion of the FSHC.

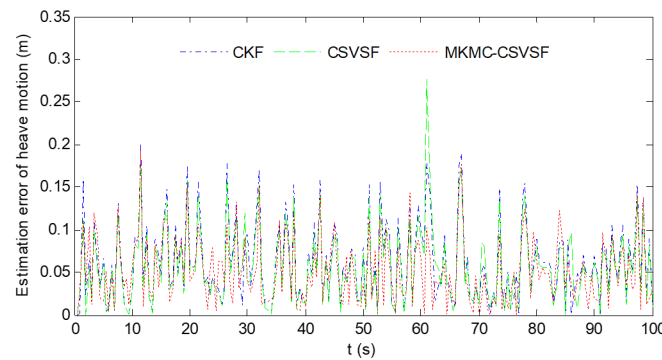


Figure 3. The estimation error of heave motion of the FSHC.

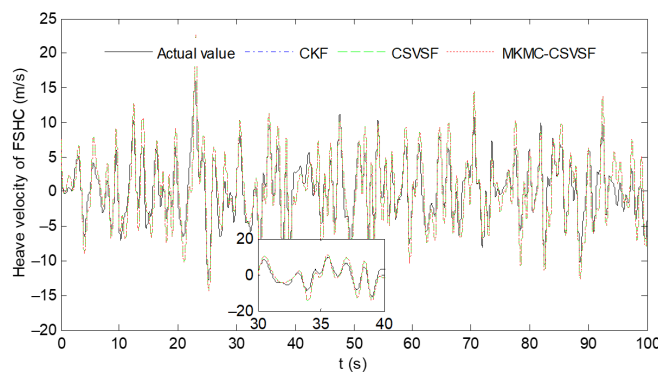
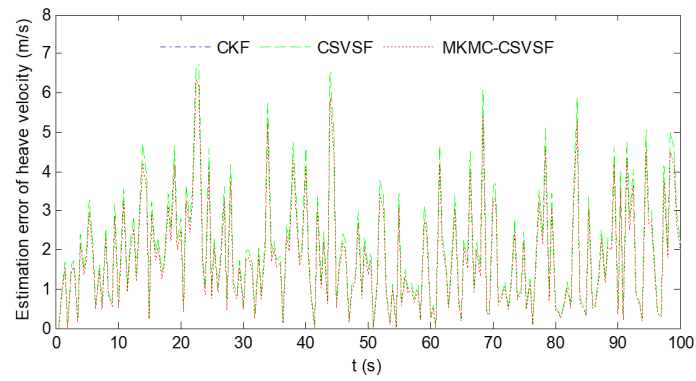
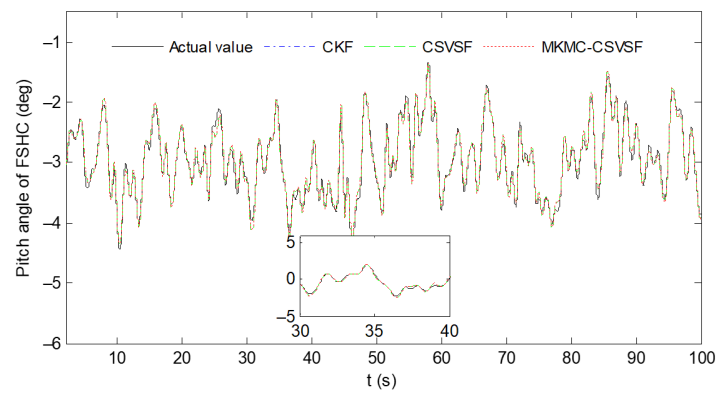


Figure 4. The estimation of heave velocity of the FSHC.



**Figure 5.** The estimation error of heave velocity of the FSHC.



**Figure 6.** The estimation of pitch angle of the FSHC.

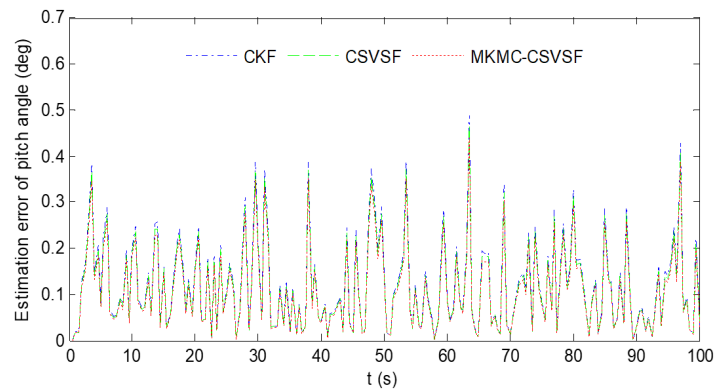


**Figure 7.** The estimation error of pitch angle of the FSHC.

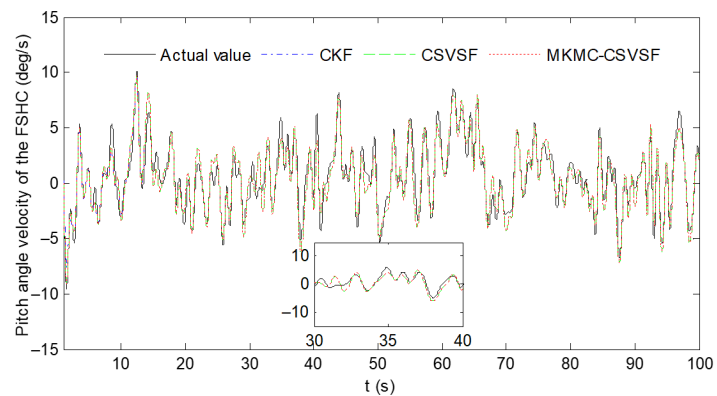


**Figure 8.** The estimation of pitch angle velocity of the FSHC.

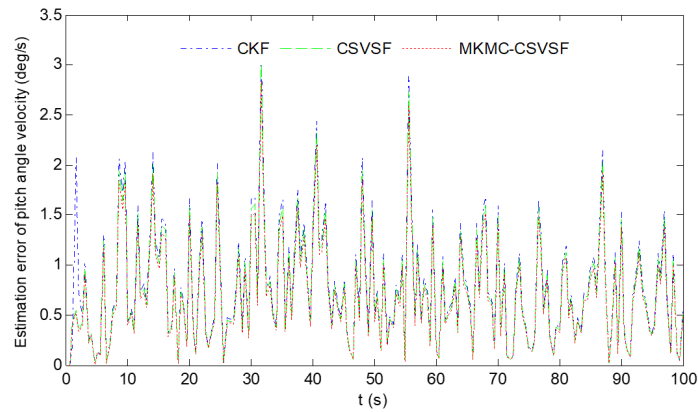


**Figure 9.** The estimation error of pitch angle velocity of the FSHC.

Moreover, the RMSE of different state estimations is shown in Figures 10–13 and the ARMSE of the MKMC-CSVSF, CSVSF and CKF of different state estimations is calculated and shown in Table 3.

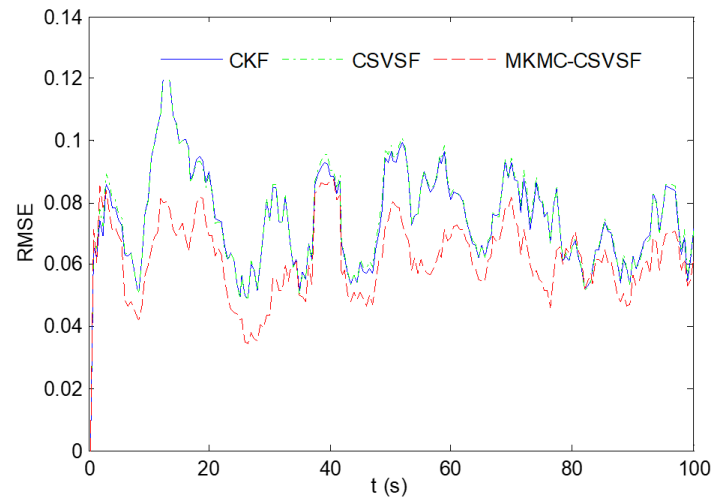


**Figure 10.** The RMSE of heave motion of the FSHC.

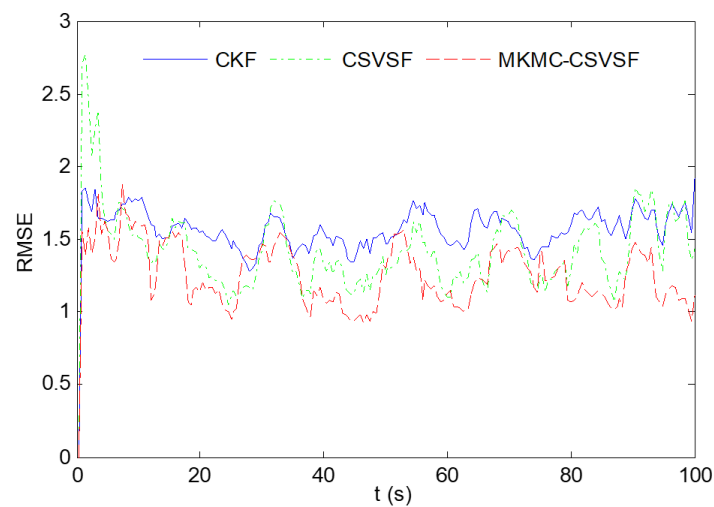


**Figure 11.** The RMSE of heave velocity of the FSHC.

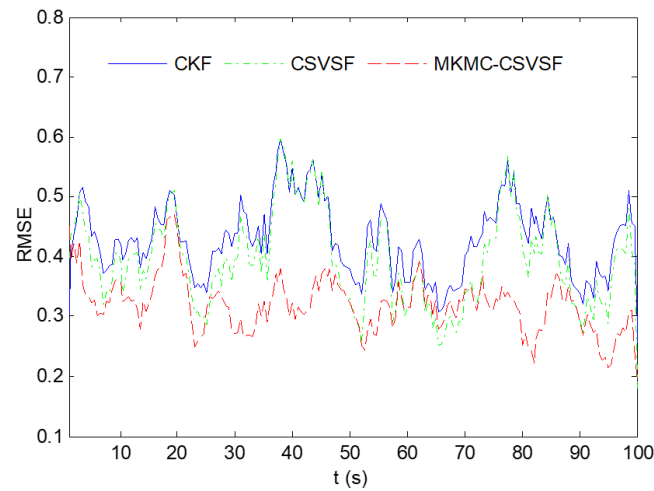


Figure 12. The RMSE of pitch angle of the FSHC.

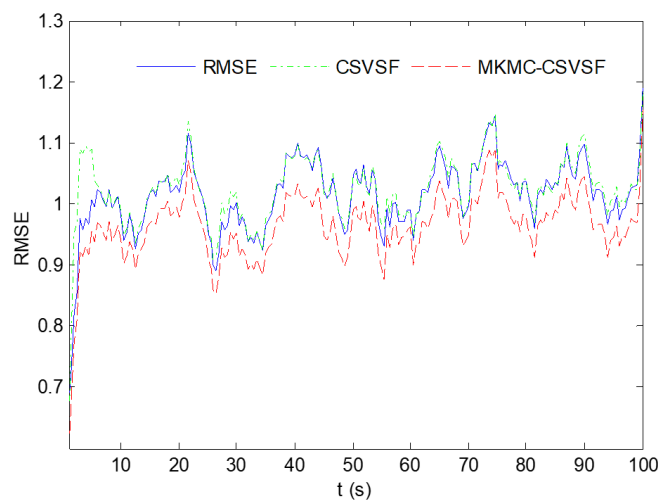


Figure 13. The RMSE of pitch angle velocity of the FSHC.

Table 3. The ARMSE of different methods.

Motion of FSHC	Filter Method		
	CKF	CSVSF	MKMC-CSVSF
Heave motion	0.1094	0.1091	0.1088
Heave velocity	2.1785	2.1422	2.0869
Pitch angle	0.6985	0.6952	0.6945
Pitch velocity	1.0272	1.0263	1.0242

Considering the evidence from the experiments presented in Figures 2–9, it can be deduced that in scenarios where heavy-tailed non-Gaussian measurement disturbances and system uncertainties are present concurrently, the MKMC-CSVSF algorithm outperforms the CSVSF and CKF methods in longitudinal motion estimation. The estimation errors associated with the MKMC-CSVSF are notably reduced in comparison to those of the CSVSF and CKF methods. The RMSE and ARMSE of the MKMC-CSVSF demonstrate a higher level of effectiveness relative to the other methodologies, as illustrated in Figures 10–13 and Table 3. Furthermore, the fuzzy rule-based selection of multi-kernel bandwidths proves to be appropriate for handling multiple kernel bandwidths, while the maximum correntropy criterion effectively addresses non-Gaussian noise scenarios. Consequently, the proposed MKMC-CSVSF performs better than the CSVSF and CKF method in the presence

of multivariate non-Gaussian noises and system uncertainties, thereby enhancing filtering accuracy and robustness against system uncertainties.

## 6. Conclusions

The MKMC-CSVSF method is presented for the state estimation with system uncertainties and heavy-tailed non-Gaussian measurement noises are proposed in this paper. The integration of the CKF and SVSF is achieved by the relationship of a constant and time-varying smooth boundary layer. Additionally, the utilization of the MKMC is introduced to improve the robustness to multivariate heavy-tailed non-Gaussian measurement noises. Furthermore, modifications to the covariance matrices in the CKF and SVSF are implemented via a fixed-point algorithm. A fuzzy rule is devised for optimal selection of kernel bandwidths. Experimental results demonstrate that the MKMC-CSVSF outperforms other methods when dealing with systems containing uncertainties and multivariate non-Gaussian noises, thereby producing notable enhancements in accuracy and robustness. Moreover, it is advisable to apply this approach in fields such as aerospace, mechanical systems, and aircraft, where heavy-tailed non-Gaussian noises are frequently encountered, to achieve accurate estimation.

**Author Contributions:** Conceptualization, H.N.; Formal analysis, S.L.; Funding acquisition, H.N.; Methodology, H.N.; Project administration, S.L.; Validation, H.N.; Writing—original draft, H.N.; Writing—review and editing, H.N. All authors have read and agreed to the published version of the manuscript.

**Funding:** This work was supported by the Natural Science Foundation of Shanxi Province (No. 2023-JC-QN-0751).

**Institutional Review Board Statement:** Not applicable.

**Informed Consent Statement:** Not applicable.

**Data Availability Statement:** Data is contained within the article.

**Conflicts of Interest:** The authors declare no conflicts of interest.

## References

1. Kalman, R.E. A New Approach to Linear Filtering and Prediction Problems. *J. Basic Eng.* **1960**, *82*, 35–45. [[CrossRef](#)]
2. Ristic, B.; Arulampalam, S.; Gordon, N. *Beyond the Kalman Filter: Particle Filters for Tracking Applications*; Artech House: Boston, MA, USA, 2004.
3. Ristic, B.; Arulampalam, S.; Gordon, N. Beyond the Kalman filter-Book Review. *Aerosp. Electron. Syst. Mag. IEEE* **2004**, *19*, 37–38. [[CrossRef](#)]
4. Arellano-Valle, R.B.; Contreras-Reyes, J.E.; Quintero, F.O.L.; Valdebenito, A. A skew-normal dynamic linear model and Bayesian forecasting. *Comput. Stat.* **2019**, *34*, 1055–1085. [[CrossRef](#)]
5. Shan-Mao, G.U.; Feng-You, H.E.; Tan, G.J.; Hui, Z. Research on Extend Kalman Filter at Low Speed in Sensorless PMSM Drives. *Electr. Drive* **2009**, *39*, 12–18.
6. Carpenter, J.; Clifford, P.; Fearnhead, P. Improved particle filter for nonlinear problems. *IEE Proc.-Adar Sonar Navig.* **2002**, *146*, 2–7. [[CrossRef](#)]
7. Eftekhari Azam, S.; Bagherinia, M.; Mariani, S. Stochastic system identification via particle and sigma-point Kalman filtering. *Sci. Iran.* **2012**, *19*, 982–991. [[CrossRef](#)]
8. Liu, X.; Guan, J.; Jiang, R.; Gao, X.; Chen, B.; Ge, S.S. Robust strong tracking unscented Kalman filter for non-linear systems with unknown inputs. *IET Signal Process.* **2022**, *16*, 351–365. [[CrossRef](#)]
9. Kolås, S.; Foss, B.A.; Schei, T.S. Constrained nonlinear state estimation based on the UKF approach. *Comput. Chem. Eng.* **2009**, *33*, 1386–1401. [[CrossRef](#)]
10. Zhang, H.; Wen, C. A Higher-Order Extended Cubature Kalman Filter Method Using the Statistical Characteristics of the Rounding Error of the System Model. *Mathematics* **2024**, *12*, 1168. [[CrossRef](#)]
11. Arasaratnam, I.; Haykin, S. Cubature Kalman Filters. *IEEE Trans. Autom. Control* **2009**, *54*, 1254–1269. [[CrossRef](#)]
12. Arasaratnam, I.; Haykin, S. Cubature Kalman smoothers. *Automatica* **2011**, *47*, 2245–2250. [[CrossRef](#)]
13. Bo, X.; Peng, Z.; Wen, H.; Xu, W. Stochastic stability and performance analysis of Cubature Kalman Filter. *Neurocomputing* **2016**, *186*, 218–227.
14. Dang, L.; Chen, B.; Huang, Y.; Zhang, Y.; Zhao, H. Cubature Kalman Filter under Minimum Error Entropy with Fiducial Points for INS/GPS Integration. *IEEE/CAA J. Autom. Sin.* **2022**, *9*, 450–465. [[CrossRef](#)]

15. Zhang, L.; Li, S.; Zhang, E.Z.; Chen, Q.W.; Guo, J. Improved square root adaptive cubature Kalman filter. *IET Signal Process.* **2019**, *13*, 641–649. [[CrossRef](#)]
16. Wan, W.K.; Feng, J.A.; Song, B.; Li, X.X. Vehicle State Estimation Using Interacting Multiple Model Based on Square Root Cubature Kalman Filter. *Appl. Sci.* **2021**, *11*, 10772. [[CrossRef](#)]
17. Zhao, J.; Mili, L. A Robust Generalized-Maximum Likelihood Unscented Kalman Filter for Power System Dynamic State Estimation. *IEEE J. Sel. Top. Signal Process.* **2018**, *12*, 578–592. [[CrossRef](#)]
18. Zhao, J. Dynamic State Estimation with Model Uncertainties Using H-infinity Extended Kalman Filter. *IEEE Trans. Power Syst.* **2018**, *33*, 1099–1100. [[CrossRef](#)]
19. Habibi, S. The Smooth Variable Structure Filter. *Proc. IEEE* **2007**, *95*, 1026–1059. [[CrossRef](#)]
20. Gadsden, S.A. Smooth Variable Structure Filtering: Theory and Applications. Ph.D. Thesis, McMaster University Library, Hamilton, ON, Canada, 2011.
21. Demim, F.; Rouigueb, A.; Nemra, A.; Bouguessa, R.; Chahmi, A. A new filtering strategy for target tracking application using the second form of Smooth Variable Structure Filter. *Proc. Inst. Mech. Eng. Part I J. Syst. Control Eng.* **2022**, *236*, 1224–1249. [[CrossRef](#)]
22. Al-Shabi, M.; Gadsden, S.A.; Habibi, S.R. Kalman filtering strategies utilizing the chattering effects of the smooth variable structure filter. *Signal Process.* **2013**, *93*, 420–431. [[CrossRef](#)]
23. Gadsden, S.A.; Al-Shabi, M.; Arasaratnam, I.; Habibi, S.R. Combined cubature Kalman and smooth variable structure filtering: A robust nonlinear estimation strategy. *Signal Process.* **2014**, *96*, 290–299. [[CrossRef](#)]
24. Tseng, C.H.; Lin, S.F.; Jwo, D.J. Robust Huber-Based Cubature Kalman Filter for GPS Navigation Processing. *J. Navig.* **2016**, *70*, 527–546. [[CrossRef](#)]
25. Wang, X.; Cui, N.; Guo, J. Huber-based unscented filtering and its application to vision-based relative navigation. *IET Radar Sonar Navig.* **2010**, *4*, 134–141. [[CrossRef](#)]
26. Wang, G.; Li, N.; Zhang, Y. Maximum correntropy unscented Kalman and information filters for non-Gaussian measurement noise. *J. Frankl. Inst.* **2017**, *354*, 8659–8677. [[CrossRef](#)]
27. Wang, G.; Zhang, Y.; Wang, X. Iterated maximum correntropy unscented Kalman filters for non-Gaussian systems. *Signal Process.* **2019**, *163*, 87–94. [[CrossRef](#)]
28. Chen, B.; Liu, X.; Zhao, H.; Principe, J.C. Maximum correntropy Kalman filter. *Automatica* **2017**, *76*, 70–77. [[CrossRef](#)]
29. Xi, L.; Hua, Q.; Jihong, Z.; Pengcheng, Y. Maximum correntropy square-root cubature Kalman filter with application to SINS/GPS integrated systems. *Isa Trans.* **2018**, *80*, 195–202.
30. Liu, X.; Ren, Z.; Lyu, H.; Jiang, Z.; Ren, P.; Chen, B. Linear and Nonlinear Regression-Based Maximum Correntropy Extended Kalman Filtering. *IEEE Trans. Syst. Man Cybern. Syst.* **2019**, *51*, 3093–3102. [[CrossRef](#)]
31. Li, S.L.; Shi, D.W.; Zou, W.L.; Shi, L. Multi-Kernel Maximum Correntropy Kalman Filter. *IEEE Control Syst. Lett.* **2022**, *6*, 1490–1495. [[CrossRef](#)]
32. Aydi, H.; Abbas, M.; Sintunavarat, W.; Kumam, P. Coincidence and fixed points for contractions and cyclical contractions in partial metric spaces. *Fixed Point Theory Appl.* **2012**, *2012*, 124. [[CrossRef](#)]
33. Liu, S.; Niu, H.; Zhang, L.; Xu, C. Modified adaptive complementary sliding mode control for the longitudinal motion stabilization of the fully-submerged hydrofoil craft. *Int. J. Nav. Archit. Ocean Eng.* **2019**, *11*, 584–596. [[CrossRef](#)]
34. Liu, S.; Niu, H.M.; Zhang, L.Y.; Guo, X.J. Adaptive compound second-order terminal sliding mode control for the longitudinal attitude control of the fully submerged hydrofoil vessel. *Adv. Mech. Eng.* **2019**, *11*, 1–13. [[CrossRef](#)]

**Disclaimer/Publisher’s Note:** The statements, opinions and data contained in all publications are solely those of the individual author(s) and contributor(s) and not of MDPI and/or the editor(s). MDPI and/or the editor(s) disclaim responsibility for any injury to people or property resulting from any ideas, methods, instructions or products referred to in the content.